Yang, L., Zare-Behtash, H., Erdem, E., and Kontis, K. (2012) Application of AA-PSP to hypersonic flows: the double ramp model. Sensors and Actuators B: Chemical, 161 (1). pp. 100-107. ISSN 0925-4005

Copyright © 2014 Elsevier B.V.

A copy can be downloaded for personal non-commercial research or study, without prior permission or charge

Content must not be changed in any way or reproduced in any format or medium without the formal permission of the copyright holder(s)

When referring to this work, full bibliographic details must be given

http://eprints.gla.ac.uk/83516

Deposited on: 18 June 2014

Enlighten – Research publications by members of the University of Glasgow
http://eprints.gla.ac.uk

Application of AA-PSP to Hypersonic Flows: The Double Ramp Model

L. Yang, H. Zare-Behtash, E. Erdem, and K. Kontis*

School of Mechanical, Aerospace and Civil Engineering, University of Manchester, UK

Abstract

Anodized Aluminium Pressure Sensitive Paint (AA-PSP) is known for its rapid response characteristics, making it a highly desirable technique when studying high-speed phenomenon on a global scale. The current study examines the efficacy of the AA-PSP technique, which is prepared with a more practical approach than that reported in literature, in analysing the flow characteristics of a double ramp model placed in hypersonic flow of M = 5. Three different flow angles of 0, -2, and -4 degrees are studied. Two-dimensional colour schlieren visualisation, using a colour wheel, is employed alongside high sensitivity Kulite pressure tap data to corroborate the AA-PSP findings. The AA-PSP results show good correlation between the qualitative schlieren and ± 8.9% discrepency with the quantitative pressure tap data. The more practical AA-PSP preparation proposed in the current study, which uses aluminium alloy 6-series rather than pure aluminium, proves it has the response time and the accuracy to be applied to unsteady high-speed flows.

*k.kontis@manchester.ac.uk.

I. INTRODUCTION

The pressure sensitive paint technique (PSP) consists of a dispersion of oxygen-sensitive photoluminescent probe molecules in an oxygen permeable binder layer.[1–3] An excitation light source of wavelength λ_e and intensity I_e excites the ruthenium molecules to higher energy state. The molecules return to their ground state via two mechanisms: (1) the emission of light at a higher wavelength, (2) the transfer of energy through collision with an oxygen molecule, a process known as dynamic or oxygen quenching.[4,5] Oxygen quenching results in a decrease in intensity of the emitted light, this process is schematically presented in Figure 1. The difference in intensities between the photoluminescent molecules at varying concentrations of O_2, and hence pressure, gives rise to the PSP method whereby luminescence can be used to determine pressure in the immediate environment.

A relatively new branch of pressure sensitive paints uses an electro-chemical process to develop a porous surface along an aluminium substrate to which the oxygen sensitive paint is added. This technique is known as Anodized Aluminium Pressure Sensitive Paint (AA-PSP).[6] The porous surface leads to an increased surface area, as shown in Figure 2, and hence, a greater chance of interaction between the oxygen molecules in the surrounding environment and the oxygen sensitive luminophore molecules in the paint.[7] Since the oxygen molecules in the flow now have a higher chance of interacting with the luminophores, the response time of the PSP is improved, enabling the measurement of unsteady flow features.

The objective of the current research is the application of AA-PSP, prepared using the more practical approach suggested in the current study, to the complicated flow over a double ramp model in hypersonic flow. Rather than anodizing pure aluminium, as is the convention in reported literature, we attempt to anodize an aluminium alloy 6-series which is more suitable for model manufacturing.

The double ramp model resembles a generic scramjet engine inlet geometry that compresses incoming flow, reduces its speed and guides it to the engine inlet with minimum spillage (shock on cowl lip condition).[8,9] However the cowl is removed for optical purposes. Understanding the flow physics associated with double ramp configurations is key in designing and optimising scramjet propulsion systems.

II. EXPERIMENTAL SETUP

A. Hypersonic tunnel

The hypersonic tunnel used in the present study is identical to that of Erdem *et. al.*[10] The tunnel is an intermediate blow-down type and uses dry air as the working fluid. The tunnel consists of a high pressure vessel, heater, settling chamber, test section, diffuser, and vacuum tank. The high pressure vessel stores dry air at 16 bars. A pneumatically operated ball valve is located between the pressure vessel and heater for quick starting. The gas temperature can be raised from ambient to sufficient high temperatures to avoid liquefaction in the test section and that of a maximum enthalpy flow condition of 700K.

A 152mm diameter axisymmetric nozzle is employed which is capable of producing a Mach 5 flow without centre body. The tunnel test section is a free-jet type with dimensions 325×325×900mm (height×width×length) having two circular quartz windows of 195mm diameter. The tunnel has a stable run time of up to 7 seconds. The variation in flow Mach number and Reynolds number for different runs of the tunnel were ± 0.4% and ± 0.3%, respectively.[10]

B. Schlieren visualisation system

The schlieren technique allows for the visualisation of otherwise invisible light refractions.[11] Conventional black and white schlieren systems utilising a slit as source and horizontal or vertical knife edge have the ability to show refractive index gradients which deflect the light rays normal to the knife edge, making the system a one-dimensional tool.[12] This presents a disadvantage when studying complicated flows e.g., where shock waves and boundary layers deflect light rays in the same direction.[13] Using two-dimensional colour schlieren systems, where a coloured wheel is placed at the knife edge location, allows for the detection of flow features that would be more difficult to identify using one-dimensional schlieren. In the present case, both black&white and colour schlieren are utilised to study the generated flow field.

A z-type schlieren system, shown in Figure 3, consisting of a continuous light source (Palflash 501) and two 8 inch diameter parabolic mirrors with 6 ft focal length is employed. The system is identical to that of Erdem *et. al.*[14] Black&white schlieren images are captured

by using a horizontal slit at the source plane and a horizontal knife edge at the cut-off plane. Colour images are acquired when the slit at the source is replaced with a circular pin hole and a 3-colour (red, blue, and green) colour wheel placed at the knife edge location, see Figure 4. A digital Canon SLR camera, EOS-450D, 12MP is used to capture the schlieren images. The camera is set to continuous shooting mode, 3.5 frames per second; the shutter speed is adjusted to a minimum value of 1/4000 seconds.

C. Testing Model

The double ramp model examined is shown in Figure 5 along with its dimensions and location of pressure taps. The model is manufactured using aluminium alloy 6-series. This material was chosen for its structural properties instead of pure aluminium.

The first ramp angle is 12 degrees and the second ramp angle is 22 degrees relative to the horizontal axis. Static pressure measurements are conducted along the model centreline at eight different locations. The pressure taps are connected to Kulite XTE-190M transducers having a range of 0 to 0.7bar. Analog signals from the transducers are acquired by a high speed data acquisition (DAQ) card, NI PCI-6251, after they are conditioned by a SXCI-1000 unit at 5kHz.

The benefit of using the double ramp model is the significant high pressure change over its surface, which is ideal for verifying PSP in hypersonic flow conditions considering the low freestream pressure level. The large pressure variations over the double ramp model also provides a greater calibration range when the AA-PSP is calibrated *in situ*.

D. AA-PSP preparation

The anodization procedure is comprised of three stages: i) pre-treatment, ii) anodization, iii) post-treatment. The pre-treatment procedure of the aluminium model adopted here is identical to that of Sakaue[15] and Kameda *et al.*[16] In the anodization part of the procedure we have adopted for a more practical approach. Where the model is to be dipped in 1 molar sulfuric acid Kameda *et al.*[16] recommends a constant temperature of 5 to $10°C$ compared to the $0°C$ used by Sakaue.[15] Since maintaining a constant low temperature requires specialist equipment, we anodize the model at room temperature, therefore eliminating the need for

temperature regulation. The post-treatment procedure of the sample is again identical to the aforementioned researchers. Figure 6 shows the SEM image of the anodized aluminium sample, the porous surface structure is evident. This figure proves that the anodization procedure can be successfully applied to the aluminium alloy 6-series, which are more suitable for manufacturing.

The solvent used to dissolve the tris-(Bathophnanthroline) Ruthenium (II) perchloride molecules was Dichloromethane (DCM). The concentration of ruthenium dissolved in DCM was 0.3mM.[17] According to Sakaue[15] DCM gives a high signal level at low pressures, this makes it the preferred solvent for the current testing conditions.

E. AA-PSP calibration procedure

PSP uses the ratio of wind-off (no flow) to wind-on (with flow) images so that the effect of paint thickness and luminophore concentration are eliminated from the intensity profiles. In the present study *in situ* calibration is used to convert the intensity ratios of the AA-PSP model into pressure maps. *In situ* calibration consists of taking pressure measurements during each run and relating the pressure values to the PSP intensity in the immediate vicinity, therefore building a relationship between PSP intensity and pressure.

In situ calibration, as opposed to *a priori* calibration, is more reliable since it eradicates any changes in calibration due to the alignment of the optical setup; this involves the location of the light source, camera, and position of the model relative to the optics. Also, because the test model is used for calibration, there is no difference between the calibration sample and testing model. By applying *in situ* calibration using the pressure taps the effects of temperature changes are minimised. In a sense, *in situ* calibration eliminates the error associated with temperature effects by absorbing it into the overall fitting error.[18]

A pair of light emitting diode (LED) panels with peak wavelength of 470nm are used for illumination. Each LED panel is comprised of an array of 13 $\times$ 10 LEDs. By using a pair of LED arrays the camera can be positioned normal to the test section with illumination from each side, leading to a uniform excitation. The advantage of placing the camera normal to the test section is that it reduces the danger of surface contamination due to internal reflections.[19] The luminescent emission was captured by a CCD camera (LaVision Image Intense) with an exposure time of 8ms.

A combination of two filters was used to capture the emitted light. The first, an orange long pass filter, only allowing the transmission of light with $\lambda > 580$nm and the second filter was an Infra-Red (IR) cut-off filter, preventing the transmission of light with $\lambda > 700$nm. The LEDs and filters were selected based on the spectral analysis of the ruthenium molecules shown in Figure 7.

III. RESULTS AND DISCUSSIONS

A. Flow Physics

When hypersonic flow passes over a two dimensional double ramp model, it is firstly compressed by the leading edge shock wave and the direction of the flow streamline turn to become parallel with the model surface. After encountering the second ramp, another shock wave is created and the flow is further compressed. At the shoulder, the flow experiences a supersonic turning via a Prandtl-Meyer expansion fan and continues along the straight region. The schematic of the flow structure can be seen in Fig. 8.

1. Theoretical analysis

Theoretical surface pressure distribution along the double ramp can be predicted using the classic inviscid oblique shock wave and Prandtl-Meyer equations. These are obtained using the free-stream Mach number and the ramp angles. The process is carried out in three stages, first the ramp angle with $\theta_1 = 12^\circ$ is examined, then the results of pressure and flow Mach number are used to solve for the second ramp $\theta_2 = 22^\circ$, finally the shoulder section of the model is analysed. Figure 8 depicts the different flow segments along with the corresponding nomenclature.

Using Eq.(1) the incidence angle of the first shock, β_1, is solved for using the free-stream Mach number, M_1, and ramp angle θ_1. Once β_1 is known the flow properties in region 2 can be found using Eqs.(2) and (3). The same procedure is applied between regions 2 and 3 across the second shock wave, originating from the second ramp, enabling the pressure and Mach number in region 3 to be determined.

$$tan\theta_1 = 2cot\beta_1 \left[\frac{M_1^2 sin^2\beta_1 - 1}{M_1^2(\gamma + cos2\beta_1) + 2}\right] \tag{1}$$

$$\frac{P_2}{P_1} = 1 + \frac{2\gamma}{\gamma + 1}(M_1^2 sin^2\beta_1 - 1) \tag{2}$$

$$M_2^2 = \frac{1}{sin^2(\beta_1 - \theta_1)} \left[\frac{M_1^2 sin^2\beta_1 + [2/(\gamma - 1)]}{[2\gamma/(\gamma - 1)M_1^2 sin^2\beta_1 - 1]}\right] \tag{3}$$

The pressure on the flat shoulder part of the model is determined theoretically from the Prandtl-Meyer function, ν, defined as:

$$\nu(M) = \sqrt{\frac{\gamma + 1}{\gamma - 1}} tan^{-1}\sqrt{\frac{\gamma - 1}{\gamma + 1}(M_i^2 - 1)} - tan^{-1}\sqrt{M_i^2 - 1} \tag{4}$$

where i refers to the locations before and after the expansion fan, regions 3 and 4 in Figure 8. Since the value of the ramp angle, θ_3, as well as the flow Mach number, M_3, are known from the above procedure, using Eqs.(5) and (6) the flow Mach number and pressure ratio on the flat shoulder of the ramp can be calculated.

$$\theta_3 = \nu(M_4) - \nu(M_3) \tag{5}$$

$$\frac{P_3}{P_4} = \left[\frac{1 + \frac{\gamma-1}{2}M_4^2}{1 + \frac{\gamma-1}{2}M_3^2}\right]^{\gamma/(\gamma-1)} \tag{6}$$

2. Flow visualisation

In the inviscid flow model, the flow will remain attached to the model surface at all times. However, when viscous effects are taken into consideration, a separation region will be formed due to the adverse pressure gradient. The separation zone starts upstream of the corner between the two ramps and reattaches on the second ramp surface. The size of separation region is a function of the magnitude of the adverse pressure gradient, surface roughness, and incoming turbulence intensity. A separation shock wave is created at the location of flow separation and a reattachment shock wave starts from the reattachment line.

The aforementioned flow structures are visualised in Figure 9 for incidence angles 0 and -4 degrees. The leading edge shock wave, separation shock, reattachment shock and Prandtl-Meyer expansion wave are clearly visible and indicated in the schlieren image. As the angle of attack is decreased from 0 to -4, the leading edge shock wave moves towards model surface in Fig. 9(b). The size of the separation region is reduced because of the relative low pressure gradient on the corner, compare to the 0 degrees case.

3. AA-PSP analysis

Figure 10 shows the relationship between intensity and pressure at each tapping location for the three incidence angles tested. The figure is known as the Stern-Volmer plot.[20] The intensity and pressure are non-dimensionalised with respect to the intensity and pressure corresponding to vacuum (reference) conditions. The intensity images of the entire model are then converted to pressure maps by applying a line of best fit to the calibration data and determining the polynomial coefficients.

Pressure mapping on the double ramp surface is presented in Fig. 11 with comparison to black&white schlieren. The small dots observed on the pressure mapping are believed to be caused by imperfections on the model surface. The AA-PSP shows the highest pressure value along the second ramp surface. This is because the flow in this region has been shocked twice, initially by the leading edge shock and afterwards by the reattachment shock. The lowest value of pressure is recorded along the shoulder due to the acceleration of the flow across the expansion fan. This behaviour is in agreement with theory.

At an incidence of 0 degrees, a curved separation zone is created before the corner. Because of this the pressure in this region is higher than the surrounding area of the first ramp.

The high pressure flow over the first ramp leaks to the sides, which is free-stream flow at a relatively lower pressure. This three-dimensional effect occurs because the double ramp does not have side walls, giving rise to the low pressure regions indicated in Fig. 11 for the 0 degree incidence case.

The pressure distribution for the -4 degrees case shows a similar pattern but at higher magnitude while the area of separation reduces. At the attachment line, some slight striation are observed which are believed to be caused by Göertler vortices due to the reattachment of

the flow on the second ramp.[21] Such complicated pressure distribution patterns are difficult to obtain using conventional pressure tapping measurement since the location of the pressure taps are fixed. This demonstrates the benefit of the AA-PSP technique for complicated flow investigations.

B. Response time

To check the response characteristics of the AA-PSP, a high speed camera (Photron SA-1) was utilised as the detector. images were captures at a rate of 2000fps with 0.5ms exposure time. Figure 12 shows the time history of the variation of AA-PSP intensity at four different tapping locations. Taps 5 and 6 are located on the second ramp whilst taps 7 and 8 are placed on the flat shoulder part of the model (see Figure 5 for tap locations). From the curve, a sudden rise of the PSP signal can be seen which corresponds to the starting process of the tunnel.

The oscillations in intensity at location of taps 5 and 6, compared to the relatively uniform intensity at taps 7 and 8, are attributed to the Göertler vortices produced from the flow reattachment on the secondary ramp surface. The ability of the AA-PSP to capture such unsteadiness demonstrates its rapid response time.

C. Comparison between different methods

Figure 13 presents the pressure profile along the centreline of the model obtained from the inviscid theory, Kulite transducers, and AA-PSP. All three methods are able to predict the general behaviour of the flow. The discrepancy between the theoretical pressure rise and AA-PSP measurements is attributed to viscous effects and the inability of the inviscid theory to predict the separation zone. Also the inviscid theory does not take into account the length-scales involved. Hence, the sudden pressure drop across the shoulder of the double ramp, where the expansion fan is present. As the AA-PSP result indicate, the pressure drop occurs over the length of the expansion fan.

Taking the pressure tap data as the 'true' value, a maximum discrepancy of $\pm$ 8.9% was found between the AA-PSP and the discrete pressure tap data.

IV. CONCLUSIONS

Using the simpler anodization procedure presented in this paper we have been able to create a porous surface on an aluminium alloy 6-series. The benefits of this research are two fold: firstly, the simpler anodization procedure eradicates the need for specialist equipment such as large ice/water baths required to maintain low temperature during anodization. This is very attractive especially when large and complicated models are studied. Secondly, aluminium alloy 6-series have better mechanical properties which are necessary for the design and manufacture of test models.

AA-PSP shows high pressure sensitivity and quick response characteristics which is required for hypersonic experiments. Application of AA-PSP on the double ramp surface captures the complicated flow regimes including curved separation zones, reattachment, and three-dimensional effects which can not be easily obtained using the conventional discreet pressure taps. The AA-PSP shows 91% agreement with the kulite pressure transducers.

Acknowledgments

The authors are indebted to the technical staff at The University of Manchester for their assistance.

---

[1] Mosharov, V., Radchenko, V., Fonov, S., "Luminescent Pressure Sensors in Aerodynamic Experiments," *Central Aerodynamic Institute (TsAGI)*, 1998.

[2] Carroll, B.F., Abbitt, J.D., Lucas, E.W., Morris, M.J., "Step Response of Pressure-Sensitive Paints," *AIAA Journal* **34**, pp. 521–526, 1996.

[3] Bell, J.H., Schairer, E.T., Hand, L.A., Mehta, D., "Surface pressure measurements using luminescent coatings," *Annual Review of Fluid Mechanics* **33**, pp. 155–206, 2001.

[4] Zare-Behtash, H., Gongora-Orozco, N., Kontis, K., Holder, S.J., "Application of novel pressure-sensitive paint formulations for the surface flow mapping of high-speed jets," *Experimental Thermal and Fluid Science* **33**, pp. 852–864, 2009.

[5] Basu, B.J., Vasantharajan, N., Raju, C., "A novel pyrene-based binary pressure sensitive paint with low temperature coefficient and improved stability," *Sensors and Actuators B: Chemical*

138, pp. 283–288, 2009.

[6] Sakaue, H., "Porous pressure-sensitive paint for characterizing unsteady flowfields," *AIAA Journal* **40**, pp. 1094–1098, 2002.

[7] Liu, T., Teduka, N., Kameda, M., Asai, K., "Diffusion timescale of porous pressure-sensitive paint," *AIAA Journal* **39**, pp. 2400–2402, 2001.

[8] Berry, S.C., Auslender, A.H., Dilley, A.D., Calleja, J.F., "Hypersonic boundary-layer trip development for Hyper-X," *Journal of Spacecraft and Rockets* **38**, pp. 853–864, 2001.

[9] Schrijer, F.F.J., Scarano, F., van Oudheusden, B.W., "Application of PIV in a Mach 7 double-ramp flow," *Experiments in Fluids* **41**, pp. 353–363, 2006.

[10] Erdem, E., Yang, L., Kontis, K., "Drag reduction by energy deposition in hypersonic flows," *16th AIAA/DLR/DGLR International Space Planes and Hypersonic Systems and Technologies Conference*, Germany, AIAA-2009-7347, 2009.

[11] Settles, G.S., "Colour-coding schlieren techniques for the optical study of heat and fluid flow," *International Journal of Heat and Fluid Flow* **6**, pp. 3–15, 1985.

[12] Settles, G.S., "Schlieren and shadowgraph techniques," *Springer Verlag*, 2001.

[13] Settles, G.S., "A direction-indicating color schlieren system," *AIAA Journal* **8**, pp. 2282–2284, 1970.

[14] Erdem, E., Yang, L., Kontis, K., "Drag Reduction Studies by Steady Energy Deposition at Mach 5," *49th AIAA Aerospace Sciences Meeting including the New Horizons Forum and Aerospace Exposition*, Orlando, AIAA-2011-1027, 2011.

[15] Sakaue, H., "Luminohpore application method of anodized aluminium pressure sensitive paint as a fast responding global pressure sensor," *Review of Scientific Instruments* **76**, pp. 1–6, 2005.

[16] Kameda, M., Tezuka, N., Hangai, T., Asai, K., Nakakita, K., Amao, Y., "Adsorptive pressure-sensitive coatings on porous anodized aluminium," *Measurement Science and Technology* **15**, pp. 489–500, 2004.

[17] Gregory, J.W., Asai, K., Kameda, M., Liu, T., Sullivan, J.P., "A review of pressure-sensitive paint for high-speed and unsteady aerodynamics," *Proceedings of the Institute of Mechanical Engineers, Part G: Journal of Aerospace Engineering* **222**, pp. 249–290, 2008.

[18] Liu, T., Sullivan, J.P., "In situ calibration uncertainty of pressure-sensitive paint," *AIAA Journal* **41**, pp. 2300–2302, 2003.

[19] Lepicovsky, J., Bencic, T.J., "Use of pressure-sensitive paint for diagnostics in turbo-machinery

flows with shocks," *Experiments in Fluids* **33**, pp. 531–538, 2002.

[20] Zelelow, B., Khalil, G.E., Phelan, G., Carlson, B., Gouterman, M., Callis, J.B., Dalton, L.R., "Dual luminophore pressure sensitive paint II. Lifetime based measurement of pressure and temperature," *Sensors and Actuators B: Chemical* **96**, pp. 304–314, 2003.

[21] Navarro-Martinez, S., Tutty, O.R., "Numerical simulation of Göertler vortices in hypersonic compression ramps," *Computers & Fluids* **34**, pp. 225–247, 2005.

List of Figures

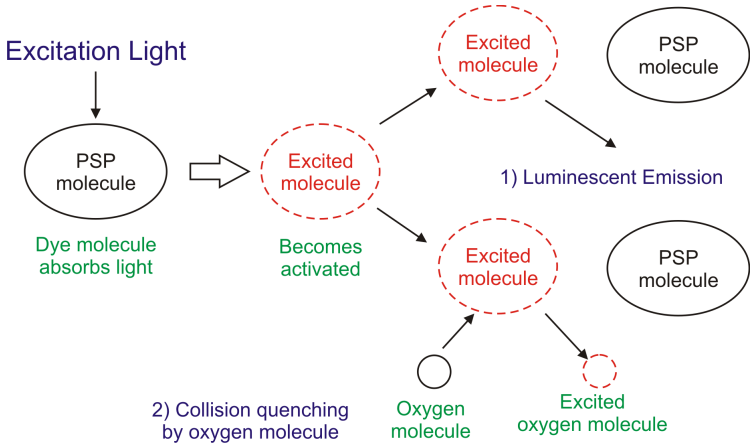

FIG. 1: Principle of PSP operation.

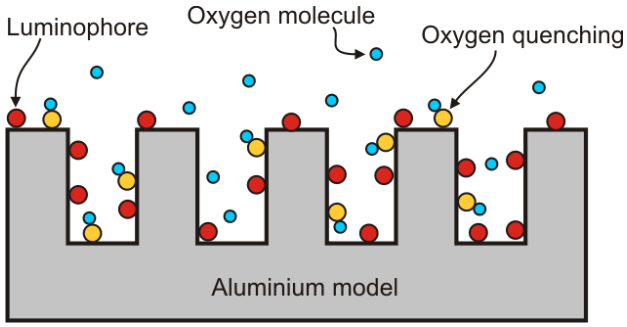

FIG. 2: Porous surface of anodized aluminium PSP.

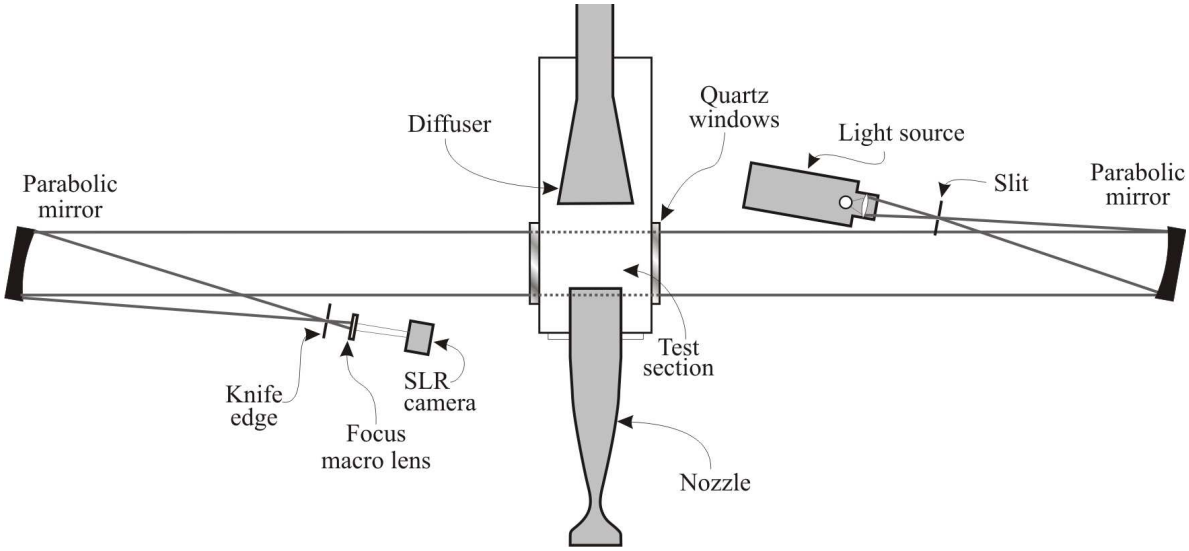

FIG. 3: Schematic of the schlieren setup.

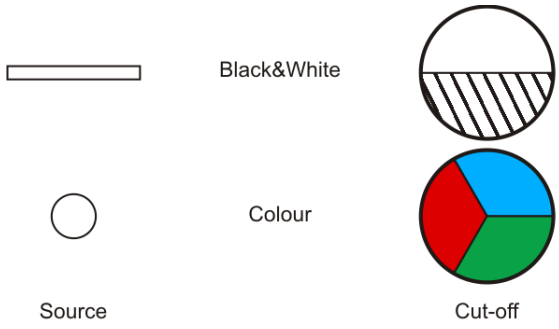

FIG. 4: Schlieren arrangements for black&white and colour methods.

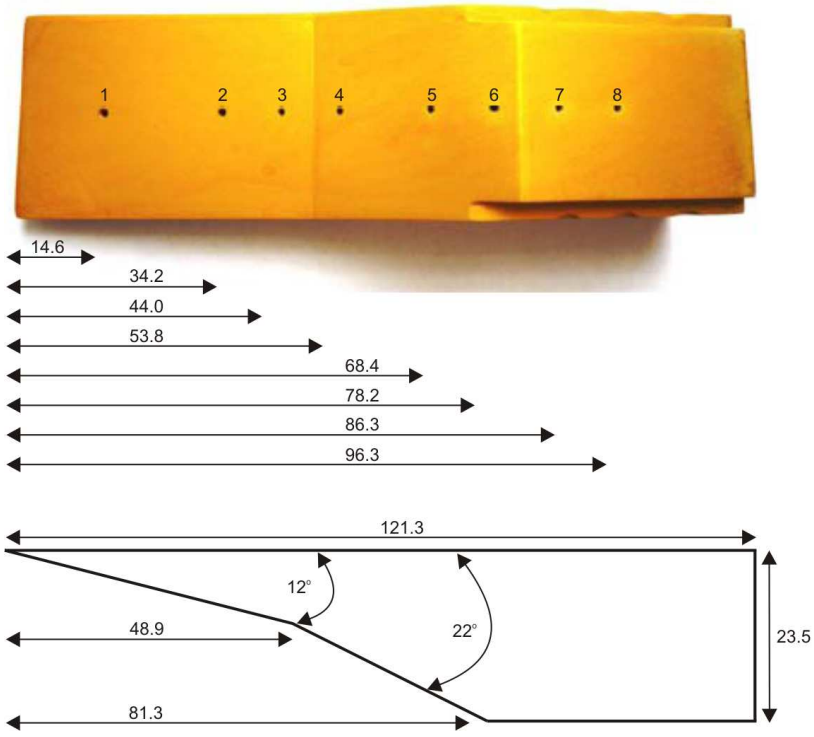

FIG. 5: Double ramp model anodized and coated with PSP, all dimensions in (mm).

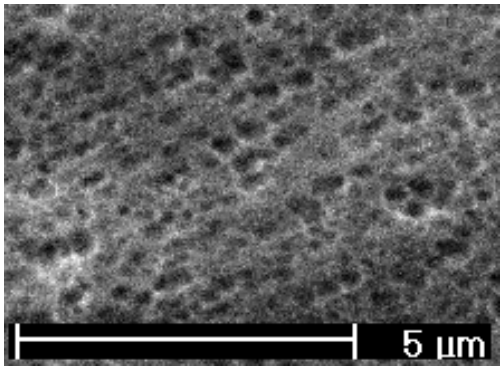

FIG. 6: SEM of anodized aluminium sample with no paint.

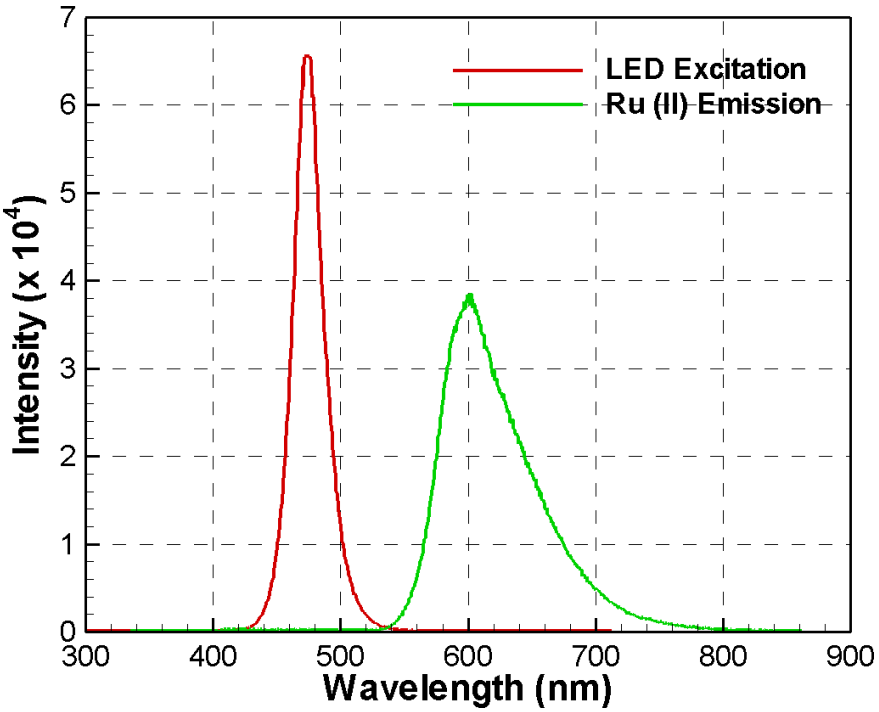

FIG. 7: Emission and excitation spectra of AA-PSP.

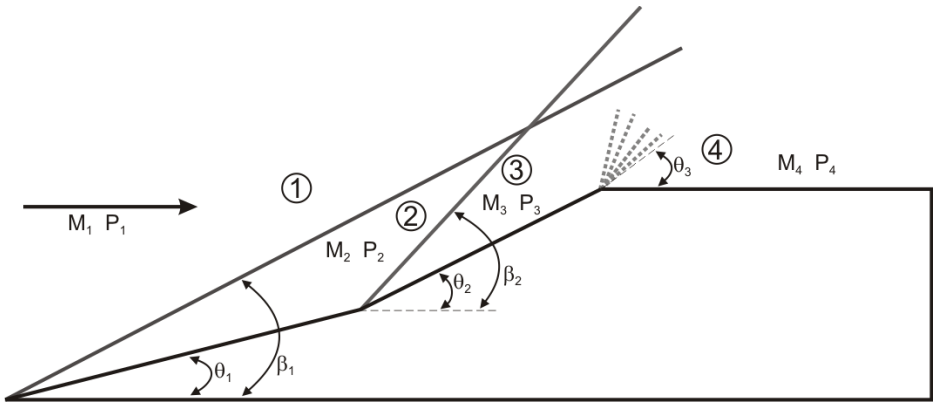

FIG. 8: Hypersonic flow over a double ramp.

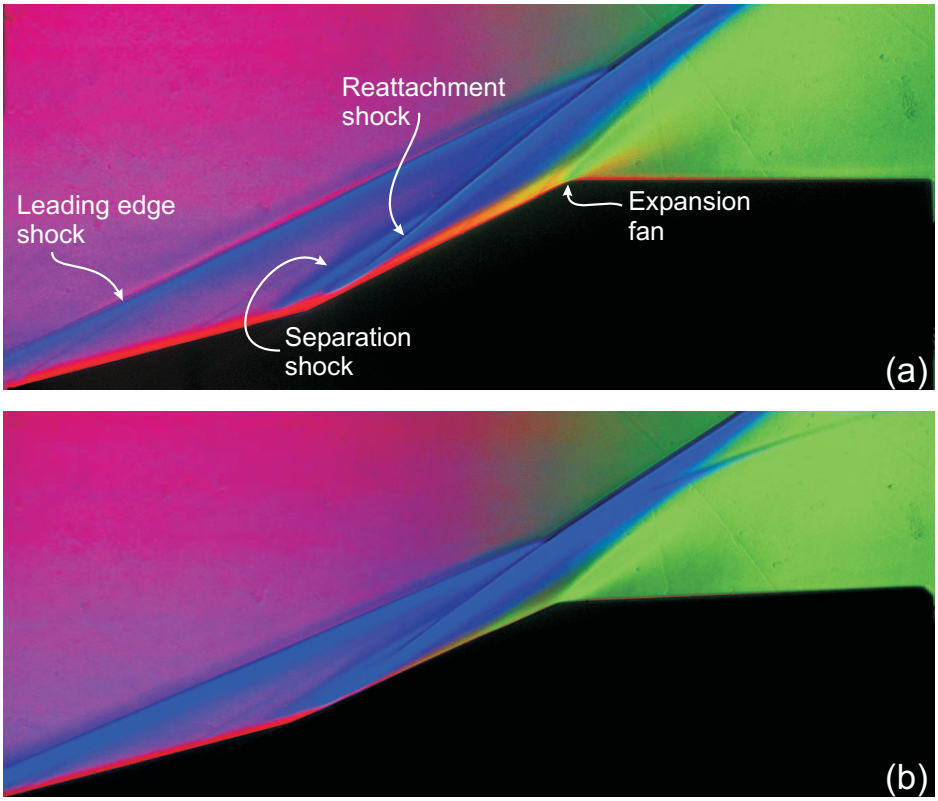

FIG. 9: Colour schlieren of the double ramp model having incidence: (a) 0 deg, (b) -4 deg.

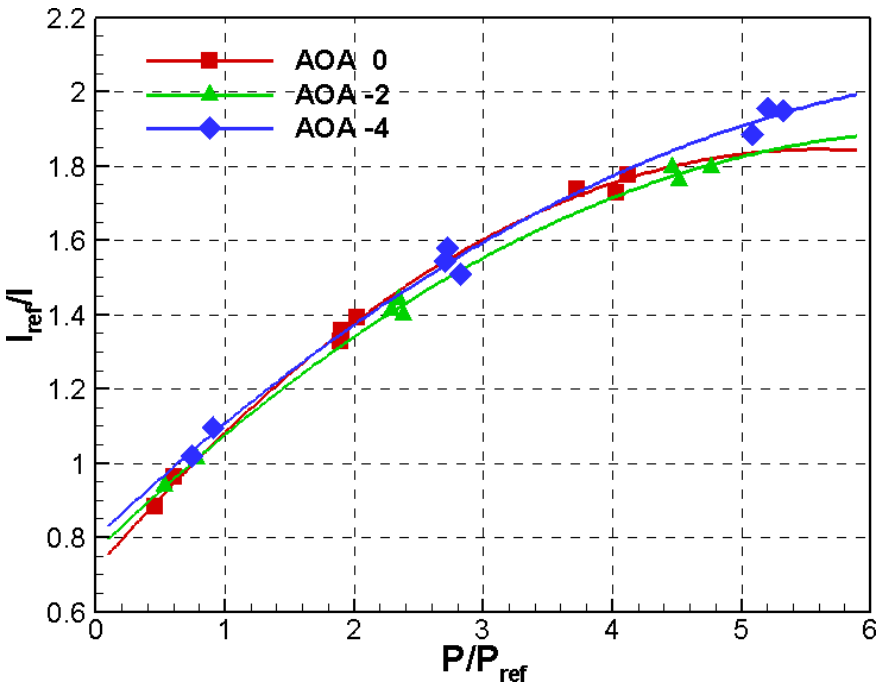

FIG. 10: Stern-Volmer plot of the AA-PSP.

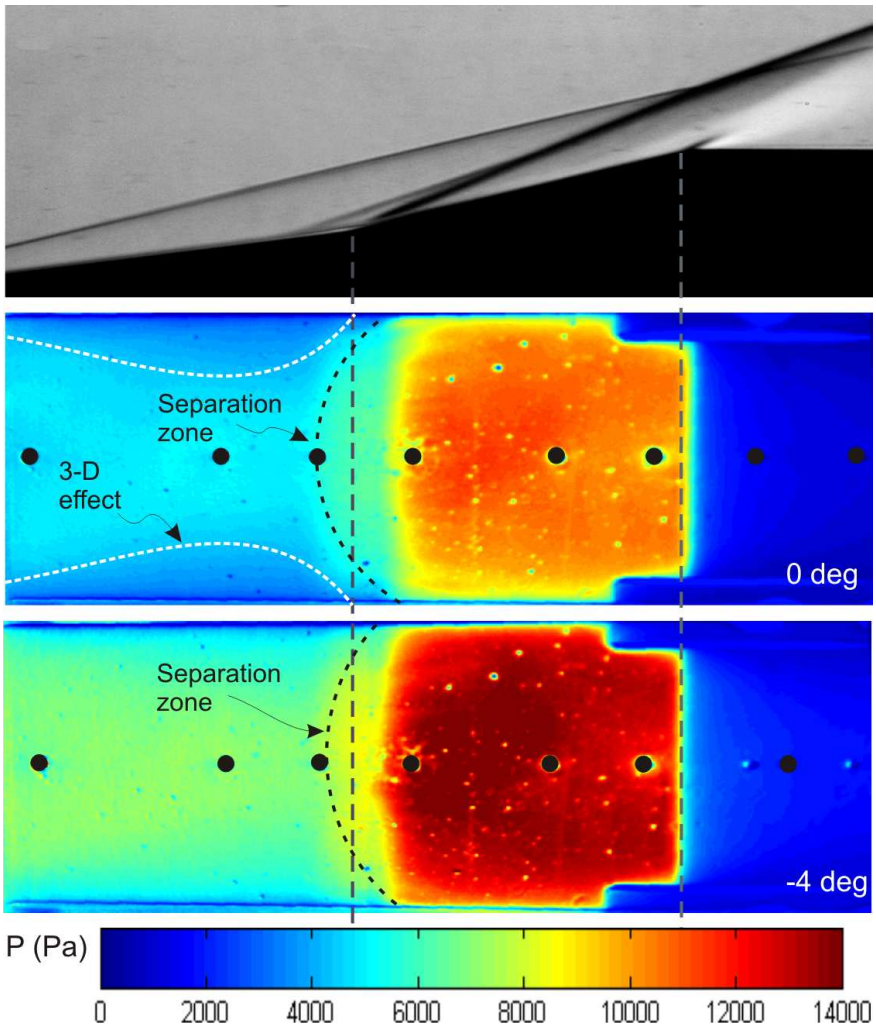

FIG. 11: AA-PSP results depicting the variation of surface pressure along the double ramp at different incidences.

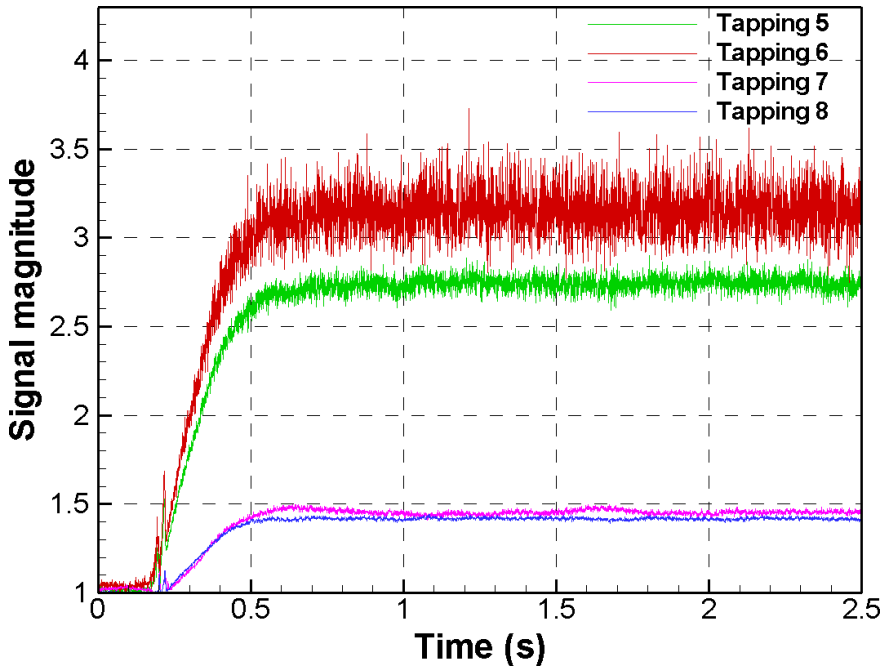

FIG. 12: Response time of AA-PSP.

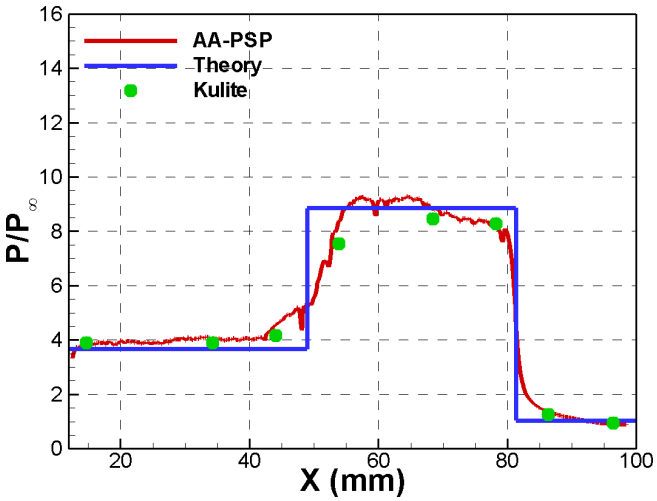

(a)

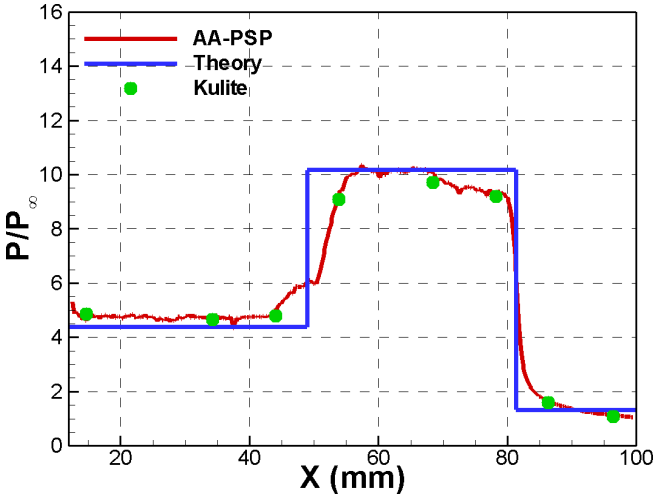

(b)

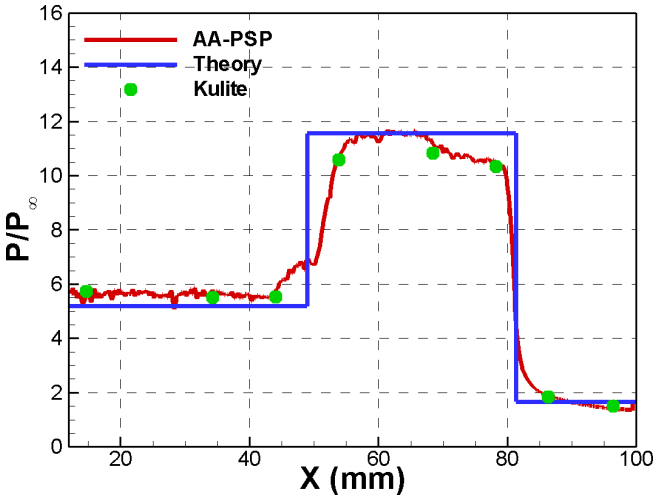

(c)

FIG. 13: Comparison between AA-PSP results with discrete pressure measurements and theory, (a) 0 deg, (b) -2 deg, (c) -4deg.